J. Chem. Sci. Vol. 123, No. 5, September 2011, pp. 755–763.

Theoretical study of the reactivity trends in the Cl-abstraction reactions of $CHCl_3 + CHX^{\cdot -}/CX_2^{\cdot -}$ (X = Cl, Br and I)

JUN XI LIANG[a], ZHI YUAN GENG[b,*] and YONG CHENG WANG[b]

[a]College of Chemical Engineering, Northwest University for Nationalities, Lanzhou, Gansu 730030, People's Republic of China

[b]Gansu Key Laboratory of Polymer Materials, College of Chemistry and Chemical Engineering, Key Laboratory of Eco-environment-related Polymer Materials; Ministry of Education, Northwest Normal University, Lanzhou, Gansu 730070, People's Republic of China

e-mail: zhiyuangeng@126.com

MS received 13 October 2010; revised 27 August 2011; accepted 8 September 2011

Abstract. To better understand how and to what extent the halosubstituted carbene radical anions effect the chlorine abstraction of $CHCl_3$, a detailed theoretical investigation has been performed at the UMP2/6-311++G (d, p)/RECP level of theory. The model system $CHCl_3 + CHX^{\cdot -}/CX_2^{\cdot -}$ (X = Cl, Br, and I) has been chosen for the present study. According to the detailed discussions of geometries and energetics of the optimized stationary points, our theoretical findings suggest that the Cl-abstraction reactions by $CHX^{\cdot -}$ are energetically favourable, indicating the less massive substitution X in $CHX^{\cdot -}$ the easier abstraction reaction, as compared to those by $CX_2^{\cdot -}$, which are energetically unfavourable and would be endothermic.

Keywords. Carbene radical anion; Cl-abstraction reaction; second-order Møller–Plesset perturbation theory (UMP2).

1. Introduction

Halocarbenes are of interest as synthetic reagents in many organic reactions[1] and their chemistry have been extensively investigated both experimentally and theoretically.[2–7] Also, their corresponding anions have received much attention, not only concerning experimental reports associated with the reactions with CH_3X (X = F, Cl, Br, I), ROH (R = CH_3, C_2H_5, $(CH_3)_2CH$, $(CH_3)_2CHCH_2$), CH_nCl_{4-n} (n = 0–3), CS_2, CSO, CO_2, O_2, CO, and N_2O,[8–10] but also involving theoretical investigations in mechanism, especially the reactions with $CHCl^{\cdot -}$ in recent years.[11,12]

Among a great deal of reactions induced by series of carbene radical anions, the reaction of $CHCl^{\cdot -} + CHCl_3$ attracts our interest. In 2008 Villano *et al*. used the flowing afterglow-selected ion flow tube instrument (FA-SIFT)[13] to probe the reaction mechanism of $CHCl^{\cdot -}$ with $CHCl_3$[10] and proposed that the reaction primarily occurs via proton transfer, and additionally by anion attack on Cl to produce $CHCl_2^-$. Note that in the Villano et al.'s experimental study the mechanism of chlorine abstraction was not suggested as compared to the mechanisms mentioned. Consequently, the present study is limited to the Cl-abstraction reaction, which stimulated their study. It should be pointed out that comparative studies are very useful in understanding similarities and differences in the chemical properties of molecules. In such cases, we present a systematic computational investigation to characterize the properties of chlorine abstraction that can be studied as a function of the substituents based on the constructed reaction model $CHCl_3 + CHX^{\cdot -}/CX_2^{\cdot -}$ (X = Cl, Br, and I) by using the conventional *ab initio* UMP2/6-311++G (d, p)/RECP level of theory.

To examine the generality of the Cl-abstraction chemistry, we shall be devoted (i) to clarify the reaction mechanism via exploring the structures and energetics of the intermediate complexes and transition states, (ii) to investigate how and to what extent the halosubstituted carbene radical anions effect the chlorine abstraction of $CHCl_3$ molecule, (iii) to compare reactivity of the $CHX^{\cdot -}$ abstraction with that of the analogous $CX_2^{\cdot -}$ abstraction, (iv) to estimate their activation barriers and to understand the origin of the barrier heights

*For correspondence

using the Activation Strain model, and (v) to finally establish general trends and predictions for the chlorine abstraction of $CHCl_3$ by $CHX^{\cdot-}/CX_2^{\cdot-}$ (Cl, Br, and I).

2. Computational methods

All equilibrium geometries in this paper have been fully optimized at the UMP2 method.[14] The large 6-311++G (d, p) basis set is performed using for H, C, Cl and Br atoms.[15] For I atom a relativistic effective core potential (RECP) (Hay and Wadt)[16] is used, also an f-type polarization function.[17] So the 4f, 5s and 5p in I is treated explicitly by a (4s4p1f) Gaussian basis set contracted to [2s2p1f]. All calculations used the RECP in which 5s and 5p electrons were treated as 'valence' electron with the remaining electrons replaced by the RECP. Frequency calculations at the same level of theory have been achieved to identify each optimized stationary point as either minima (the number of imaginary frequencies (NIMAG = 0)) or transition-state structures (NIMAG = 1) and to evaluate the zero-point energy (ZPE) corrections, which are included in all relative energies. Moreover, the transition states corresponding to both the reactants and the products direction in the reaction pathways were examined by using the intrinsic reaction coordinate (IRC).[18] Furthermore, the natural population analysis (NPA) has been made in terms of natural bond orbital (NBO) method.[19] All calculations reported here have been carried out with GAUSSIAN 03[20] program package.

3. Results and discussion

Before the presentation of the calculated results for those Cl-abstraction reactions, it is perhaps worthwhile to describe briefly the mechanisms of the title reactions. As shown in figure 1, a double-well PES can be displayed in their mechanisms as vividly expressed as follows: reactants (Rea) → precursor complex (Cpx) → transition state (TS) → radical intermediate (Rim) → products (Pro). To simplify the comparisons and to emphasize the trends, we have given their energies relative to the two reactant molecules, i.e., $CHX^{\cdot-}/CX_2^{\cdot-}$ + $CHCl_3$, which are listed in table 1. The major conclusions drawn from the current study can be summarized as follows.

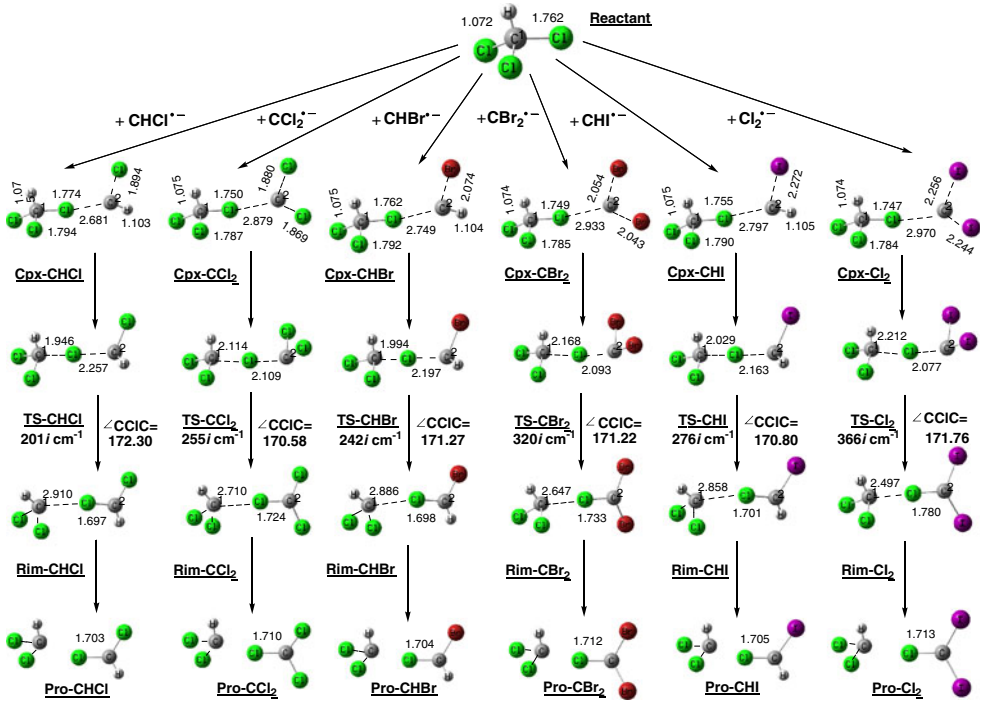

Figure 1. Optimized geometries of Cl-abstraction reactions of $CHCl_3$ with $CHX^{\cdot-}/CX_2^{\cdot-}$ (X = Cl, Br and I) at the UMP2/6-311++G (d, p)/RECP level of theory, the bond distance of reactants $CHX^{\cdot-}$ and $CX_2^{\cdot-}$ ($CHCl^{\cdot-}$ [C–H: 1.120; C–Cl: 1.892], $CHBr^{\cdot-}$ [C–H: 1.121; C–Br: 2.064], $CHI^{\cdot-}$ [C–H: 1.121; C–I: 2.253], $CCl_2^{\cdot-}$ [C–Cl: 1.871], $CBr_2^{\cdot-}$ [C–Br: 2.046], $CI_2^{\cdot-}$ [C–I: 2.238]), with bond distances in Å and angles in degree.

Table 1. Relative energy E_r (kJ mol^{-1}) and spin density S_d in C^1 and C^2 atoms of all geometries of Cl-abstraction reactions.

System	E_r	C^1 atom with S_d	C^2 atom with S_d
Rea-CHCl	0.00	0.000	1.079
Rea-CHBr	0.00	0.000	1.066
Rea-CHI	0.00	0.000	1.045
Rea-CCl_2	0.00	0.000	1.000
Rea-CBr_2	0.00	0.000	0.989
Rea-CI_2	0.00	0.000	0.976
Cpx–CHCl	−33.66	−0.012	1.093
Cpx–CHBr	−29.43	−0.008	1.082
Cpx-CHI	−26.61	−0.008	1.066
Cpx-CCl_2	−19.50	−0.005	1.003
Cpx–CBr_2	−15.77	−0.004	0.994
Cpx–CI_2	−13.98	−0.003	0.985
TS-CHCl	−27.52	0.141	0.878
TS-CHBr	−16.62	0.216	0.788
TS-CHI	−7.37	0.262	0.751
TS-CCl_2	17.97	0.484	0.472
TS-CBr_2	35.76	0.497	0.508
TS-CI_2	46.63	0.503	0.603
Rim-CHCl	−85.54	−0.005	0.907
Rim-CHBr	−63.46	−0.007	0.904
Rim-CHI	−44.93	−0.005	0.897
Rim-CCl_2	10.57	−0.004	0.828
Rim-CBr_2	29.86	−0.010	0.799
Rim-CI_2	41.44	−0.032	0.752
Pro-CHCl	−65.19 (−65.20)[a]	0.000	0.921
Pro-CHBr	−41.85 (−41.69)[a]	0.000	0.920
Pro-CHI	−23.33 (−22.87)[a]	0.000	0.921
Pro-CCl_2	40.32 (56.25)[a]	0.000	0.818
Pro-CBr_2	76.89 (83.61)[a]	0.000	0.811
Pro-CI_2	102.25 (99.65)[a]	0.000	0.803

[a]Values in parentheses denote the $\Delta_r H_m^\theta$ at 298 K

3.1 *Precursor complexes*

As expected, the weakly bound intermediate complexes for the reactions, $CHCl_3 + CHX^{\cdot-}/CX_2^{\cdot-}$ (X = Cl, Br and I), are initially formed. Calculated vibrational frequencies for the ion-dipole complexes reveal that their structures are true minima on the potential energy surfaces (PES). According to our computations as given in figure 1, the precursor complexes (Cpx–CHCl, Cpx–CHBr, Cpx-CHI, Cpx–CCl_2, Cpx–CBr_2 and Cpx–CI_2) all display very similar $C^2HX/C^2X_2^{\cdots}C^1HCl_3$ bonding characteristics. More intriguing, the calculated C^1–Cl^* bond distance (the Cl^* denotes the abstracted chlorine) is lengthed by 0.7% in Cpx–CHCl, unchanged in Cpx–CHBr, shortened by 0.4% in Cpx-CHI, and uniformly shortened by 0.7–0.9% in Cpx-CX_2 (X = Cl, Br and

Table 2. Computed NBO charges (a.u.) at the UMP2/6-311++G (d, p)/RECP level.

	Rea			Cpx			TS				Pro	
X^1X^2	$C^2X^1X^{2\cdot-}$	Cl^*	C^1HCl_2	$C^2X^1X^2$	Cl^*	C^1HCl_2	$C^2X^1X^2$	Cl^*	C^1HCl_2	$[Cl^*]$-$[C^2]$	$Cl^*C^2X^1X^{2\cdot}$	$C^1HCl_2^-$
HCl	−1.000	0.029	−0.029	−0.889	0.109	−0.221	−0.659	−0.009	−0.332	0.474	0.000	−1.000
HBr	−1.000	0.029	−0.029	−0.919	0.119	−0.199	−0.627	−0.034	−0.339	0.479	0.000	−1.000
HI	−1.000	0.029	−0.029	−0.936	0.121	−0.185	−0.611	−0.047	−0.342	0.535	0.000	−1.000
ClCl	−1.000	0.029	−0.029	−0.961	0.121	−0.160	−0.584	−0.128	−0.335	0.160	0.000	−1.000
BrBr	−1.000	0.029	−0.029	−0.976	0.116	−0.141	−0.535	−0.112	−0.378	0.307	0.000	−1.000
I I	−1.000	0.029	−0.029	−0.983	0.114	−0.131	−0.516	−0.095	−0.389	0.517	0.000	−1.000

I), respectively, while the other C^1–Cl bond distance is completely stretched by 1.8%, 1.7%, 1.6%, 1.4%, 1.3% and 1.2% in Cpx–CHCl, Cpx–CHBr, Cpx-CHI, Cpx-CCl_2, Cpx–CBr_2 and Cpx–CI_2, respectively, compared to the C^1–Cl equilibrium bond length in isolated $CHCl_3$. The reasons for such a difference can be traced to charge transfer as reported in table 2. Our theoretical calculations suggest that the trend in charges transferred also mirrors the trend in C^1–Cl bond length change: Cpx–CHCl (0.111 a.u.) > Cpx–CHBr (0.081 a.u.) > Cpx-CHI (0.064 a.u.) and Cpx-CCl_2 (0.039 a.u.) > Cpx–CBr_2 (0.024 a.u.) > Cpx–CI_2 (0.017 a.u.). In addition, the quantitative analysis has been provided to account for the correlation of degree of charge transfer in the Cpxs with bond length change of C^1–Cl^* from the Reactants to corresponding Cpxs. As shown in figure 2, there are two good linear correlations for Cpx-CHX (R = 0.985) and for Cpx-CX_2 (R = 0.922), respectively, indicating the extent of bond distance change is associated with the degree of charge transfer, suggesting similar bond change arises in Cpx-CX_2 than in Cpx-CHX, where X = Cl, Br and I. Obviously, it is a critical point that the charge transferred of 0.081 a.u. in Cpx, i.e., from reactants to corresponding precursor complexes, the C^1–Cl^* is lengthened when the charge transferred is above 0.081 a.u., while analogous C^1–Cl^* is shortened if the charge transferred is below 0.081 a.u.. Furthermore, it should be noted that the length of the σ C^1–Cl^* bond decreases in the order Cpx–CHCl (1.774 Å) > Cpx–CHBr (1.762 Å) > Cpx-CHI (1.755 Å), but closes as Cpx-CCl_2 (1.750 Å) ≈ Cpx–CBr_2 (1.749 Å) ≈ Cpx–CI_2 (1.747 Å). Presumably this is due to the existence of conjugated Πp-bond in CX_2 fragment, further indicating less charge transfer take place in Cpx-CX_2 than in Cpx-CHX. This bonding effect is also reflected that the C^2–X bond distances of Cpx-CX_2 are shorter than analogous those of Cpx-CHX, as indicated in figure 1.

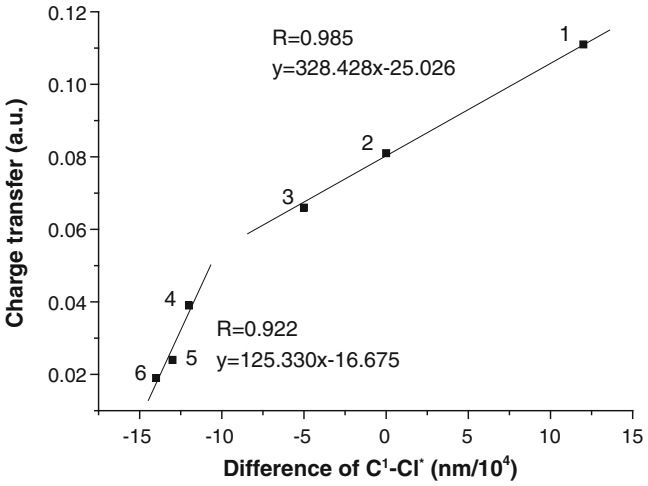

Figure 2. Correlations of charges transfer with difference of C^1–Cl^* bond distances. The Cpxs (1, Cpx–CHCl [0.111, 12]; 2, Cpx–CHBr [0.081, 0]; 3, Cpx-CHI [0.064, −3]; 4, Cpx-CCl_2 [0.039, −12]; 5, Cpx–CBr_2 [0.024, −13]; 6, Cpx–CI_2 [0.017, −15]).

On the other hand, the complexation energies obtained for the ion-molecule complexes, at the UMP2/6-311++G (d, p)/RECP level of theory, are uniformly negative and increases in the order (kJ mol^{-1}) Cpx–CHCl (−33.66) < Cpx–CHBr (−29.43) < Cpx-CHI (−26.61) and Cpx-CCl_2 (−19.50) < Cpx–CBr_2 (−15.77) < Cpx–CI_2 (−13.98), as observed from table 1. Notably, the formation of all complexes do not need to conquer any energy barriers and corresponding stabilization decreases as X varies from Cl to Br to I, and in this case, the Cpx-CHX complexes possess higher stabilization than the Cpx-CX_2 complexes. Moreover, the difference in stability of these adducts is easily understood in terms of the HOMO (Lewis base; i.e., $CHX^{\cdot-}$/$CX_2^{\cdot-}$)–LUMO (Lewis acid; i.e., $CHCl_3$) interaction. According to the perturbation theory,[21–25] both a smaller HOMO–LUMO gap and a larger overlap between them results in a greater Lewis adduct stabilization. According to our theoretical investigations, we note that the energy of the HOMO decreases in the order (kJ mol^{-1}) $CHCl^{\cdot-}$ (−136.53) > $CHBr^{\cdot-}$ (−162.78) > $CHI^{\cdot-}$ (−170.71) and $CCl_2^{\cdot-}$ (−254.67) > $CBr_2^{\cdot-}$ (−267.80) > $CI_2^{\cdot-}$ (−286.24). In other words, a less massive substitution X results in a greater Cpx stabilization in which the stability of Cpx-CHX are higher than that of Cpx-CX_2.

3.2 *Transition states*

Starting from the stable precursor complexes, we have successfully located the transition states (TS-CHCl, TS-CHBr, TS-CHI, TS-CCl_2, TS-CBr_2 and TS-CI_2) for the abstraction reactions, and all TSs were confirmed to be first-order saddle points with only one imaginary frequency. Examination of the single imaginary frequency for each transition state (201*i* cm^{-1} for TS-CHCl, 242*i* cm^{-1} for TS-CHBr, 276*i* cm^{-1} for TS-CHI, 255*i* cm^{-1} for TS-CCl_2, 320*i* cm^{-1} for TS-CBr_2, and 366*i* cm^{-1} for TS-CI_2) provides excellent confirmation of the concept of the abstraction process, primarily the C–Cl bond in $CHCl_3$ stretching with Cl atom migrating to the carbon center of $CHX^{\cdot-}$/$CX_2^{\cdot-}$. This is fully borne out by our IRC computations, as seen from figure 3. Indeed, the pronounced similarity among those

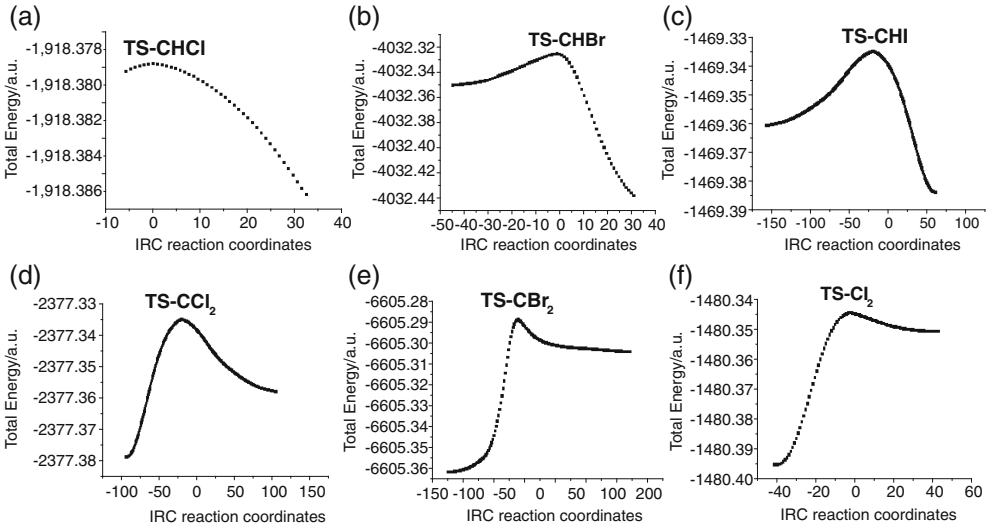

Figure 3. Potential energy profiles along the coordinate.

Table 3. Activation strain analysis of the activation barriers relative to precursor complexes.[a]

	$\Delta E^{\neq}$	$\Delta E^{\neq}_{\text{strain}}$	$\Delta E^{\neq}_{\text{int}}$
TS-CHCl	6.14	32.59	−26.45
TS-CHBr	12.81	57.36	−44.55
TS-CHI	19.24	76.65	−57.41
TS-CCl_2	37.47	123.82	−86.35
TS-CBr_2	51.53	142.08	−90.55
TS-CI_2	60.61	152.93	−92.32

[a]Values are reported in kJ mol^{-1} at the UMP2 level

Table 4. NBO analysis for the transition-state structures for the reactions of the mono- and dihalosubstituted species.[a]

	σ_{donor}	$\sigma^*_{\text{acceptor}}$	$E(2)$ (kJ mol^{-1})	ΔE(a.u.)	F_{ij}(a.u.)
C^2HCl-Cl^*-C^1HCl_2	$\sigma_{C^2\text{-}Cl}$	$LP^*_{Cl^*}$	0.67	1.42	0.019
C^2HBr-Cl^*-C^1HCl_2	$\sigma_{C^2\text{-}Br}$	$LP^*_{Cl^*}$	1.84	1.35	0.031
C^2HI-Cl^*-C^1HCl_2	$\sigma_{C^2\text{-}I}$	$LP^*_{Cl^*}$	3.03	1.19	0.038
C^2Cl_2-Cl^*-C^1HCl_2	$\sigma_{C^2\text{-}Cl}$	$LP^*_{Cl^*}$	1.92	1.55	0.034
C^2Br_2-Cl^*-C^1HCl_2	$\sigma_{C^2\text{-}Br}$	$LP^*_{Cl^*}$	2.93	1.37	0.039
C^2I_2-Cl^*-C^1HCl_2	$\sigma_{C^2\text{-}I}$	$LP^*_{Cl^*}$	4.11	1.22	0.045

[a]$E(2)$ is the perurbative analysis hyperconjuagtive energy, ΔE is the energy difference between the σ and σ^* NBOs, and F_{ij} is the Fock matrix element between the NBOs i and j

transition states is the near linear three-center pattern involving a chlorine atom and two carbon atoms. As seen from figure 1, the C^1–Cl^*–C^2 bond angles for the mono- and dihalosubstituted TS structures range 170.80–172.30° and 170.58–171.76°, respectively. Moreover, our theoretical results also presented some periodic trends in TS structures as given in figure 1. For instance, the C^1–Cl^* internuclear separations for the monochloro-, bromo-, and iodo-substituted transition states are in the order TS-CHCl (1.946 Å) < TS-CHBr (1.994 Å) < TS-CHI (2.029 Å). Additionally, the same trend is predicted for the disubstituted transition states TS-CCl_2 (2.114 Å) < TS-CBr_2 (2.168 Å) < TS-CI_2 (2.212 Å). These values suggest that the Cl-abstraction reaction with lighter halosubstituted carbene radical anion takes place earlier along the reaction coordinate. Thus, the TS of the reaction by $CHCl^{\cdot-}$ has stronger reactant-like character than those of the others. According to the Hammond postulate,[26] the TS-CHCl should have the smallest and TS-CI_2 the highest activation barriers. This was fully confirmed by our theoretical calculations. As shown in table 3, the barrier height from the corresponding precursor complex increases in the order (kJ mol^{-1}) TS-CHCl (6.14) < TS-CHBr (12.81) < TS-CHI (19.24) and TS-CCl_2 (37.47) < TS-CBr_2 (51.53) < TS-CI_2 (60.61). In other words, the closer the X atom is to the end of a group, the higher the chlorine abstraction conquers barrier. Comparatively, the distance of the C^2 and Cl^* atoms shows also similar trends upon mono- and disubstitution TSs by chlorine, bromine, and iodine atoms, that is, TS-CHCl (2.257 Å) > TS-CHBr (2.197 Å) > TS-CHI (2.163 Å) and TS-CCl_2 (2.109 Å) > TS-CBr_2 (2.093 Å) > TS-CI_2 (2.077 Å). Those are ascribed to the electrostatic repulsion between the negatively charged C^2 and Cl^* atoms. As indicated in table 2, our UMP2 calculations suggest that the difference in negative charges between Cl^* and C^2 increases in the order (a.u.) TS-CHCl (0.474) < TS-CHBr (0.479) < TS-CHI (0.535) and TS-CCl_2 (0.160) < TS-CBr_2 (0.307) < TS-CI_2 (0.517). Moreover, as reflected in NBO analysis for the TS structures as indicated in table 4, the difference in the donor abilities supported by the energy of $\sigma_{C^2\text{-}X} \rightarrow LP^*_{Cl^*}$ interaction increase in the order (for monosubstituted TSs) $\sigma_{C^2\text{-}Cl} \rightarrow LP^*_{Cl^*}\left(0.67\,kJ\,mol^{-1}\right) < \sigma_{C^2\text{-}Br} \rightarrow LP^*_{Cl^*}\left(1.84\,kJ\,mol^{-1}\right) < \sigma_{C^2\text{-}I} \rightarrow LP^*_{Cl^*}\left(3.03\,kJ\,mol^{-1}\right)$. The same trend applies to the disubstituted TS structures $\sigma_{C^2\text{-}Cl} \rightarrow LP^*_{Cl^*}\left(1.92\,kJ\,mol^{-1}\right) < \sigma_{C^2\text{-}Br} \rightarrow LP^*_{Cl^*}\left(2.93\,kJ\,mol^{-1}\right) < \sigma_{C^2\text{-}I} \rightarrow LP^*_{Cl^*}\left(4.11kJ\,mol^{-1}\right)$. Also, these trends reflect those of charges transferred from C^2HX/C^2X_2 moieties, which increase in the order (a.u.) TS-CHCl (0.341) < TS-CHBr (0.373) < TS-CHI (0.389) and TS-CCl_2 (0.416) < TS-CBr_2 (0.465) < TS-CI_2 (0.484), as seen from table 2. This is in accordance with the result[27] that a later TS would allow more charges to transfer. Hence, our theoretical calculations suggest that the ease of chlorine migration at the TS states for both mono- and dihalosubstituted reactions decreases as substitution X goes down the group and TS-CHX exhibit more preferential chlorine migration than corresponding TS-CX_2. On the basis of above discussions, one may therefore conclude that chlorine abstraction of the title reactions ($CHCl_3$ + $CHX^{\cdot-}/CX_2^{\cdot-}$) is increasing difficult as substitution X varies from Cl to I. Besides, the model calculations also suggest the Cl-abstraction reactions of $CHX^{\cdot-}$ are usually more favourable than those of $CX_2^{\cdot-}$.

To better understand the reactivity among 6 reaction processes, we have analysed their activation barriers using the Activation Strain model[28–32] in which the activation energy $\Delta E^{\neq}$ is decomposed into the activation strain $\Delta E^{\neq}_{strain}$ and the stabilizing transition state (TS) interaction $\Delta E^{\neq}_{int}$ between the reactants in the activated complex: $\Delta E^{\neq} = \Delta E^{\neq}_{strain} + \Delta E^{\neq}_{int}$. In this paper, we choose the system of $CHCl_3 + CHCl^{\cdot-}$ as an illustrative example to explain our Activation Strain model and the other studied systems are analogous. For the system of $CHCl_3 + CHCl^{-}$, the activation strain $\Delta E^{\neq}_{strain}$ refers to the relative energy of the total energy of the deformed reactants ($CHCl_3 + CHCl^{-}$) in geometry of activated complex with that of Cpx–CHCl and corresponding transition state interaction $\Delta E^{\neq}_{int}$ is the relative energy of the total energy of the deformed reactants with that of corresponding TS-CHCl. All results of the Activation Strain analysis are listed in table 3. Comparisons of the $\Delta E^{\neq}_{strain}$ and $\Delta E^{\neq}_{int}$ components in TSs reveal that the $\Delta E^{\neq}_{strain}$ for both Cpx-CHX and Cpx-CX_2 demonstrate a same trend as increase in the order: TS-CHCl < TS-CHBr < TS-CHI and TS-CCl_2 < TS-CBr_2 < TS-CI_2, but the $\Delta E^{\neq}_{int}$ obviously show decreased behaviour as follows, TS-CHCl > TS-CHBr > TS-CHI and TS-CCl_2 > TS-CBr_2 > TS-CI_2, and the net result is that the $\Delta E^{\neq}$ exhibit the orders of $CHCl^{\cdot-} + CHCl_3$ < $CHBr^{\cdot-} + CHCl_3$ < $CHI^{\cdot-} + CHCl_3$ and $CCl_2^{\cdot-} + CHCl_3 < CBr_2^{\cdot-} + CHCl_3 < CI_2^{\cdot-} + CHCl_3$. Obviously, in this case $\Delta E^{\neq}_{int}$ is not the decisive factor of activation energy. Furthermore, as known that the origin of activation strain is directly related to the bond strength of the activated bond[33] which may be expressed by the percentage-wise extent of bond stretching in TS. This is fully confirmed by our theoretical calculations. As shown in figure 4, there are two good linear correlations

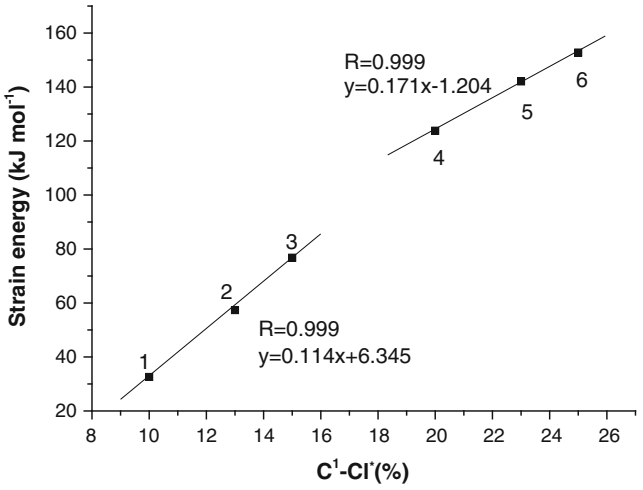

Figure 4. Correlations of strain energy $\Delta E^{\neq}_{\text{strain}}$ with C^1–Cl^* bond strength for the Cl-abstraction reactions. The TSs (1, TS-CHCl [32.59, 10]; 2, TS-CHBr [57.36, 13]; 3, TS-CHI [76.65, 15]; 4, TS-CCl_2 [123.82, 20]; 5, TS-CBr_2 [142.08, 23]; 6, TS-CI_2[152.93, 25]).

of $\Delta E^{\neq}_{\text{strain}}$ with the strength of C^1–Cl^* bond, indicating the same R (0.999) in the mono- and disubstituted transition states. Thus, we conclude that the Cl^* transfer ability derives directly from the strength of C^1–Cl^* bond activated by $CHX^{\cdot-}/CX_2^{\cdot-}$, in other words, a longer C^1–Cl^* bond distance need to suffer a higher energy barrier because of a higher destabilizing substrate strain.

3.3 *Radical intermediates*

Along the pathways, as shown in figure 1, the corresponding product intermediates $C^1HCl_2^{\cdots}Cl^*C^2HX/Cl^*C^2X_2$ (Rim-CHCl, Rim-CHBr, Rim-CHI, Rim-CCl_2, Rim-CBr_2 and Rim-CI_2) are yielded. As expected, the structures of the complexes are found to be more similar to those of final products. Indeed, the C^2–Cl^* bonds were already formed for each product intermediate. Our UMP2 calculations indicate that the distance of formed C^2–Cl^* bond is 1.697, 1.698, and 1.701 Å for Rim-CHCl, Rim-CHBr, and Rim-CHI and 1.724, 1.733, and 1.780 Å for Rim-CCl_2, Rim-CBr_2, and Rim-CI_2, respectively. Moreover, the Rim-CHX complexes should possess higher stabilization than the Rim-CX_2 complexes. For instance, the UMP2 results estimate that the energies of Rim-CHCl, Rim-CHBr, and Rim-CHI are below those of the reactants by 85.54, 63.46, and 44.93 kJ mol^{-1}, respectively, whereas the energies of Rim-CCl_2, Rim-CBr_2, and Rim-CI_2 are above those of the reactants by 10.57, 29.86, and 41.44 kJ mol^{-1}, respectively. On these basis, we further confirm that the Cl-abstraction reactions by $CHX^{\cdot-}$ are more favourable than those by $CX_2^{\cdot-}$.

3.4 *Products*

The optimized structures (Pro-CHCl, Pro-CHBr, Pro-CHI, Pro-CCl_2, Pro-CBr_2 and Pro-CI_2) are collected in figure 1. Our theoretical results reveal that all products consist of two sections, that is, $C^1HCl_2^{\cdot-}$ with strongly pyramidal structure and $Cl^*C^2HX^{\cdot}/Cl^*C^2X_2^{\cdot}$ with nearly planar geometry. Here, especially it may be noted that the newly formed C^2–Cl^* bonds in TSs relative to their final equilibrium values are lengthened by a range of 33%-27% for $CHX^{\cdot-}$ abstractions and 23%-21% for $CX_2^{\cdot-}$ abstractions, respectively. These features strongly suggest that the $CHX^{\cdot-}$ abstraction reactions reach the TS relatively early compared to the $CX_2^{\cdot-}$ abstraction reactions which arrive at the TS relatively late. Thus, one may anticipate a larger exothermicity for the reactions by $CHX^{\cdot-}$, which is further confirmed by our spin density (S_d) analysis. As shown in table 1, for six Cl-abstractions, the S_d in C^2 for either precursor or radical complexes uniformly demonstrates the same trend as the order of C^2 ($CHCl^{\cdot-}$) > C^2 ($CHBr^{\cdot-}$) > C^2 ($CHI^{\cdot-}$) > C^2 ($CCl_2^{\cdot-}$) > C^2 ($CBr_2^{\cdot-}$) > C^2 ($CI_2^{\cdot-}$). Presumably the instability for both precursor and radical complexes would follow a monotonic increase from *Complex* ($CHCl^{\cdot-}$) to *Complex* ($CHBr^{\cdot-}$) to *Complex* ($CHI^{\cdot-}$) to *Complex* ($CCl_2^{\cdot-}$) to *Complex* ($CBr_2^{\cdot-}$) to *Complex* ($CI_2^{\cdot-}$) because the investigated system is an ion-dipole complex. This is not inconsistent with the known result,[34] proposing the systems with the lowest S_d is the most stable. More importantly, the S_d values given above in $CHX^{\cdot-}$ abstractions are bigger than those in $CX_2^{\cdot-}$ abstractions. So, it is reasonable if we consider the exothermic for $CHX^{\cdot-}$ reactions and the endothermic for $CX_2^{\cdot-}$ reactions.[27] There is also, for example, a clear trend in reaction enthalpies $\Delta_r H^{\theta}_m$ (298 K) that can be observed in table 1 for the monosubstituted reactions are in the order (kJ mol^{-1}) Pro-CHCl (−65.20) < Pro-CHBr (−41.69) < Pro-CHI (−22.87). The same trend is predicted for the disubstituted reactions (kJ mol^{-1}) Pro-CCl_2 (56.25) < Pro-CBr_2 (83.61) < Pro-CI_2 (99.65). Here, the reaction enthalpy (−65.20 kJ mol^{-1}) obtained for the reaction of $CHCl^{\cdot-}$ with $CHCl_3$ is in good agreement with the experimental data (≈−66.94 kJ mol^{-1}),[10] indicating our computational approach introduced should be rationally adapted to this investigative system. In addition, although $CHX^{\cdot-}$ reactions are predicted to undergo exothermic

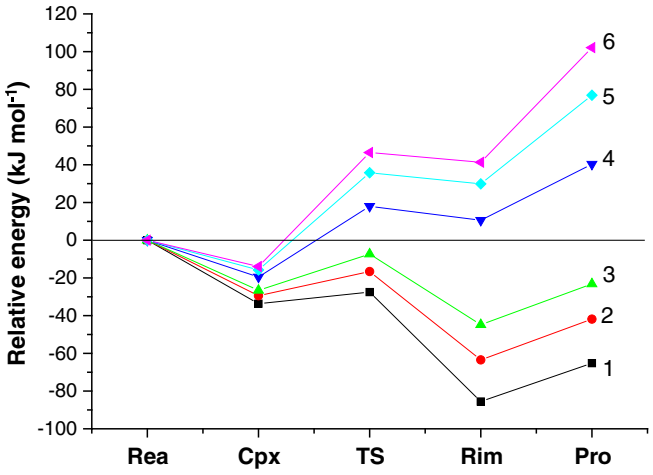

Figure 5. Energy profiles for the Cl-abstraction reactions of substrate $CHCl_3$ with both $CHX^{\cdot-}$ and $CX_2^{\cdot-}$. The pathways (1, $CHCl^{\cdot-}$ + $CHCl_3$; 2, $CHBr^{\cdot-}$ + $CHCl_3$; 3, $CHI^{\cdot-}$ + $CHCl_3$; 4, $CCl_2^{\cdot-}$ + $CHCl_3$; 5, $CBr_2^{\cdot-}$ + $CHCl_3$; 6, $CI_2^{\cdot-}$ + $CHCl_3$), the relative energies are taken from the UMP2/6-311++G (d, p)/RECP level of theory as given in table 1.

abstractions whereas $CX_2^{\cdot-}$ reactions endothermic processes as shown above, from figure 5 it can be noted that the energies for both $CHX^{\cdot-}$ and $CX_2^{\cdot-}$ abstraction reactions present a great similarity in trend, which is borne out by our UMP2 calculations. Considering entropy factor is nearly equal in the reactant and products, so relative energy E_r description is introduced in next discussion. As shown in table 1, the E_r order of $CHX^{\cdot-}$ abstractions that also follows the trend in activation energy is (kJ mol^{-1}) Pro-CHCl (−65.19 kJ) < Pro-CHBr (−41.85) < Pro-CHI (−23.33), which supports the prediction that the activation barrier should be correlated to the exothermicity.[35,36] Likewise, the endothermicity for the $CX_2^{\cdot-}$ abstractions is predicted to be in the order (kJ mol^{-1}) Pro-CHCl (40.32) < Pro-CHBr (76.89) < Pro-CHI (102.25), indicating that the abstraction reactions induced by $CX_2^{\cdot-}$ are energetically unfavourable.

4. Conclusion

In summary, to gain insight into the essence of the Cl-abstraction reactions of $CHCl_3$ with $CHX^{\cdot-}/CX_2^{\cdot-}$ (X = Cl, Br, and I), a detailed theoretical investigation has been provided with *ab initio* calculations at UMP2/6-311++G (d, p)/RECP level of theory. With the above analysis in mind, the following conclusion can be drawn: (i) all the reaction model proceed via a double-well PES involving a central barrier and a transition state. (ii) The formation of the initial encounter complexes are uniformly spontaneous and barrierless processes, when $CHX^{\cdot-}/CX_2^{\cdot-}$ approaches $CHCl_3$. (iii) Using the activation strain model analysis, it is inferred that $\Delta E_{int}^{\neq}$ can not dominate the activation barriers of the Cl-abstraction reactions. (iv) The reactivity of the title reactions increase as the order of $CHI^{\cdot-}$ + $CHCl_3$ < $CHBr^{\cdot-}$ + $CHCl_3$ < $CHCl^{\cdot-}$ + $CHCl_3$ and $CI_2^{\cdot-}$ + $CHCl_3$ < $CBr_2^{\cdot-}$ + $CHCl_3$ < $CCl_2^{\cdot-}$ + $CHCl_3$, where the reactions by $CHX^{\cdot-}$ exhibit more activity than those by $CX_2^{\cdot-}$.

Acknowledgements

The authors wish to acknowledge the support received from The Natural Science Foundation of Gansu province (Grant No. 0710RJZA114), The Natural Science Foundation of Gansu province education office (Grant No.0801-10), The Person with Ability Introduce and Scientific Research Item of Northwest University for Nationalities.

References

1. Rablen P R, Paiz A A, Thuronyi B W and Jones M J 2009 *J. Org. Chem.* **74** 4252
2. Tao C, Reid S A, Schmidt T W and Kable S H 2007 *J. Chem. Phys.* **126** 51105
3. Mukarakate C, Tao C, Jordan C D, Polik W F and Reid S A 2008 *J. Phys. Chem. A* **112** 466
4. Krogh-Jespersen K, Yan S and Moss R A 1999 *J. Am. Chem. Soc.* **121** 6269
5. Hancock G, Ketley G W and MacRobert A J 1984 *J. Phys. Chem.*, **88** 2104
6. Za'rate A O, Martinez R, Rayo M N S, Castano F and Hancock G 1992 *J. Chem. Soc. Faraday Trans.* **88** 535
7. Browsword R A, Hancock G and Oum K W 1996 *J. Phys. Chem.* **100** 4840
8. Born M, Ingemann S and Nibbering N M M 1994 *J. Am. Chem. Soc.* **116** 7210
9. Villano S M, Eyet N, Lineberger W C and Bierbaum V M 2009 *Int. J. Mass. Spectrom.* **12** 280
10. Villano S M, Eyet N, Lineberger W C and Bierbaum V M 2008 *J. Am. Chem. Soc.* **130** 7214
11. Li Y, Liu H-L, Sun Y-B, Li Z, Huang X-R and Sun C-C 2010 *J. Phys. Chem. A* **74** 84
12. Li Y, Liu H-L, Zhou Z-J, Sun Y-B, Li Z, Huang X-R and Sun C-C 2010 *J. Mol. Struct: THEOCHEM.* **114** 953
13. Van Doren J M, Barlow S E, Depuy C H and Bierbaum V M 1987 *Int. J. Mass. Spectrom.* **81** 85
14. Hehre W J, Radom L, Schleyer P V R and Pople J A 1986 *Ab initio molecular orbital theory* (New York: Wiley)
15. Takahashi M, Tsutsui S, Sakamoto K, Kira M, Muller T and Apeloig Y 2001 *J. Am. Chem. Soc.* **123** 347
16. Hay P and Wadt W R 1985 *J. Chem. Phys.* **82** 299
17. Neuhaus A, Frenking G, Huber C, Gauss J 1992 *Inorg. Chem.* **31** 5355

18. Fukui K 1981 *Acc. Chem. Res.* **14** 363
19. Reed A E, Curtiss L A and Weinhold F 1988 *Chem. Rev.* **88** 899
20. Frisch M J, Trucks G W and Schlegel H B et al. 2003 Gaussian 03, Gaussian Inc., USA, Pittsburgh PA.
21. Moss R A, Fedorynski M and Shieh W-C 1979 *J. Am. Chem. Soc.* **101** 4736
22. Moss R A and Munjal R C 1979 *Tetrahedron Lett.* **19** 4721
23. Smith N P and Stevens I D R 1979 *J. Chem. Soc. Perkin. Trans.* **2** 1298
24. Moss R A 1980 *Acc. Chem. Rev.* **13** 58
25. Jones W M, LaBar R A, Brinker U H, Gebert P H 1977 *J. Am. Chem. Soc.* **99** 6379
26. Hammond G S 1954 *J. Am. Chem. Soc.* **77** 334
27. McKee M L 1997 *J. Org. Chem.* **62** 7942
28. Blowers P, Ford L and Masel R 1998 *J. Phys. Chem. A* **102** 9267
29. Diefenbach A and Bickelhaupt F M 2001 *J. Chem. Phys.* **115** 4030
30. Diefenbach A and Bickelhaupt F M 2004 *J. Phys. Chem. A* **108** 8460
31. Kavitha K and Venuvanalingam P 2005 *Int. J. Quant. Chem.* **67** 104
32. Ess D H and Houk K N 2008 *J. Am. Chem. Soc.* **130** 10187
33. Diefenbach A and Bickelhaupt F M 2004 *J. Phys. Chem. A* **108** 8460
34. Yadav P, Mohan H, Maity D K, Suresh C H and Rao B S M 2008 *Chem. Phys.* **57** 351
35. Su M-D and Chu S-Y 1999 *J. Am. Chem. Soc.* **121** 4229
36. Su M-D and Chu S-Y 1999 *Tetrahedron Lett.* **40** 4371